VERSITA

Biologia **69**/1: 1—9, 2014
Section Cellular and Molecular Biology
DOI: 10.2478/s11756-013-0290-3

Identification of critical amino acid residues for chloride binding of *Bacillus licheniformis* trehalose-6-phosphate hydrolase

Ping-Lin Ong[1]*, Tzu-Ting Chuang[1,2]*, Tzu-Fan Wang[3] & Long-Liu Lin[2]**

[1] *Department of Biochemical Science and Technology, National Chiayi University, 300 Syuefu Road, Chiayi County 60004, Taiwan*
[2] *Department of Applied Chemistry, National Chiayi University, 300 Syuefu Road, Chiayi County 60004, Taiwan; e-mail: llin@mail.ncyu.edu.tw*
[3] *Department of Chemistry, National Cheng Kung University, Tainan City 701, Taiwan*

Abstract: Based on sequence alignment of selected Cl^- dependent and independent glycoside hydrolase family 13 enzymes, two invariant residues (Arg201 and Asn347) and one tyrosine (Tyr365) that might be responsible for the binding of *Bacillus licheniformis* trehalose-6-phosphate hydrolase (*Bl*TreA) to chloride ion were identified. The role of these three residues was further explored by mutational and biophysical analyses. The mutant enzymes (R201Q/E/K, N327Q/D/K, and Y365A/R) and *Bl*TreA were individually overexpressed in *Escherichia coli* M15 host cells and purified by one-step nickel affinity chromatography on Ni-NTA resin. The purified *Bl*TreA and Y365A had a specific activity of 236.9 and 47.6 U/mg protein, respectively. The remaining enzymes lost their hydrolase activity completely even in the presence of high salt. With the exception of Y365A, all mutant enzymes did not have the ability to bind fluoride, chloride and nitrate anions. Structural analyses showed that the circular dichroism spectra of the mutant proteins were consistent with those of *Bl*TreA. However, wild-type and mutant enzymes displayed a slight difference in the profiles of intrinsic tryptophan fluorescence. Collectively, these results clearly indicate that Arg201 and Agr327 residues might play an essential role in chloride binding of *Bl*TreA.

Key words: *Bacillus licheniformis*; trehalose-6-phosphate hydrolase; site-directed mutagenesis; chloride binding; arginine.

Abbreviations: *Bc*Ogl, *Bacillus cereus* oligo-1,6-glucosidase; *Bl*TreA, *Bacillus licheniformis* trehalose-6-phosphate hydrolase; CD, circular dichroism; GH, glycoside hydrolase; IPTG., isopropyl-β-D-thiogalactopyranoside; LB, Luria-Bertani; MRW, mean residue weight; Ni-NTA, nickel-nitrilotriacetate; *p*NP, *p*-nitrophenol; *p*NPG, *p*-nitrophenyl-α-D-glucopyranoside; PPA, porcine pancreatic α-amylase; SDS-PAGE, sodium dodecyl sulphate-polyacrylamide gel electrophoresis.

Introduction

The α-amylase family comprises a considerable number of starch hydrolases and related enzymes (MacGregor 1993; Janeček 1994; Svensson 1994) with about 20 different substrate specificities, and is currently termed glycoside hydrolase (GH) family 13 (Henrissat 1991; Henrissat & Bairoch 1996). Three-dimensional structures of several GH13 family enzymes, including α-amylases (Matsuura et al. 1984; Brady et al. 1991; Qian et al. 1993; Kadziola et al. 1994; Brayer et al. 1995; Machius et al. 1995; Ramasubbu et al. 1996), cyclodextrin glucanotransferases (Klein & Schulz 1991; Kubota et al. 1991; Lawson et al. 1994; Knegtel et al. 1996), and oligo-1,6-glucosidase (Kizaki et al. 1993; Watanabe et al. 1997) are already available. Collectively, family GH13 enzymes have certain criteria of evolution conservatory: (1) a very low degree of sequence similarities, located at or near strands β2, β3, β4, β5, and β7, and at a short region close to the C-terminus of domain B, serving as fingerprints (Kizaki et al. 1993; Knegtel et al. 1996); (2) an insertion of domain B between strand β3 and helix α3 of the catalytic $(\beta/\alpha)_8$-barrel (MacGregor 1993; Janeček 1994; Svensson 1994); and (3) three fully conserved catalytic residues Asp206, Glu230, and Asp297 (numbering as in Taka-amylase A) (Qian et al. 1994; Strokopytov et al. 1995).

Despite the catalytic activities of most GH13 enzymes are independent of chloride ion, this anion has been shown to induce an allosteric activation in a bacterial α-amylase (Feller et al. 1992; Feller et al. 1994). Removal of Cl^- definitely leads to a complete loss of the enzymatic activity, which is fully recovered by the incorporation of Cl^- and Br^- ions into the apo-enzyme (Feller et al. 1996). The chloride ion binding site for Cl^--dependent mammalian pancreatic and salivary α-amylases consists of Arg195, Asn298, Arg337, and a water molecule (Qian et al. 1993; Brayer et al. 1995;

* Ping-Lin Ong and Tzu-Ting Chuang contributed equally to this work
** Corresponding author

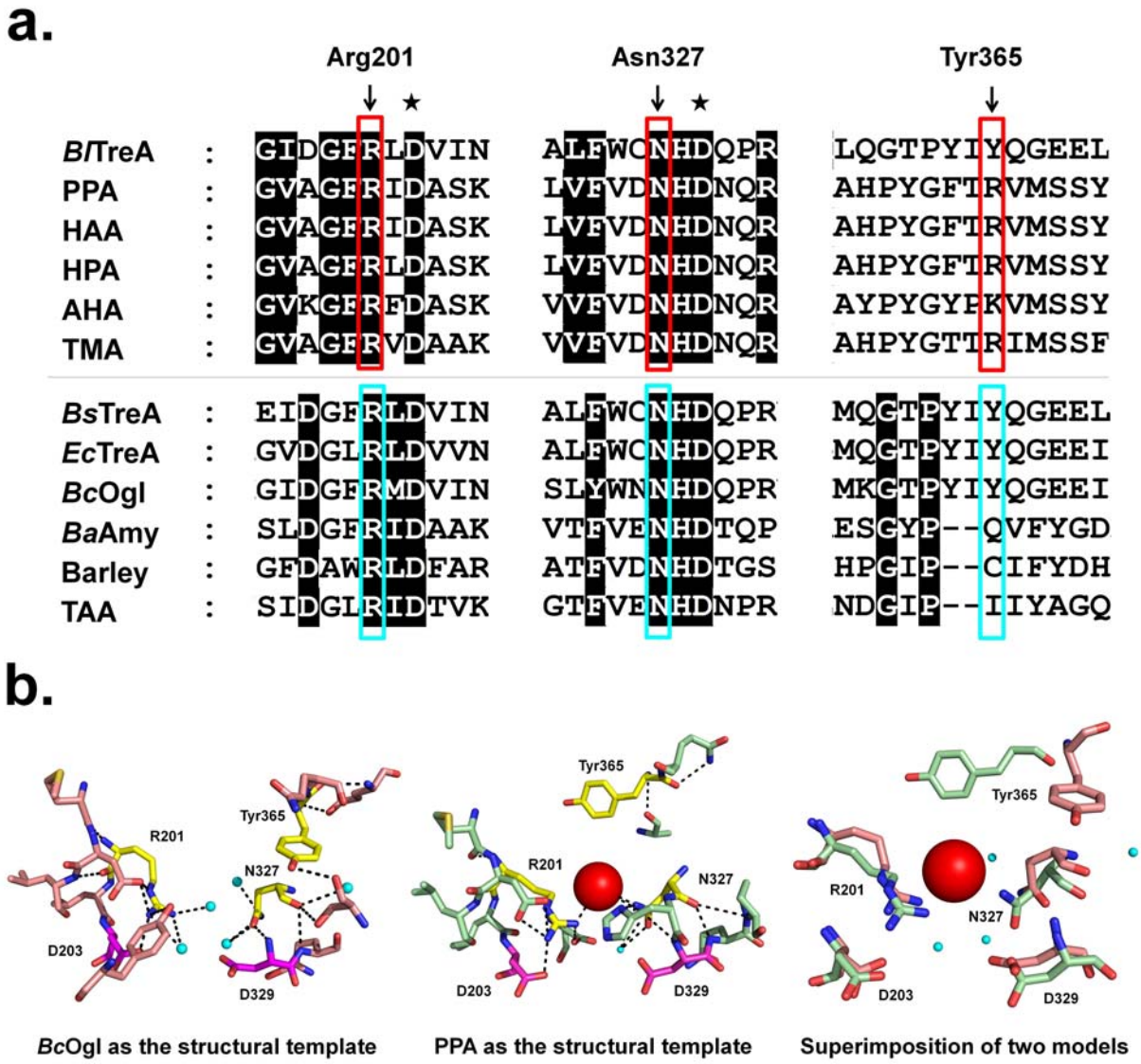

Fig. 1. Sequence alignment of *Bl*TreA with other counterparts and the putative Cl^--binding site of the enzyme. (a) Alignment of homologous regions bearing the chloride ligands. Gaps in aligned sequences (dashes) were included to maximize protein similarities. Protein ligands of the chloride-binding site are boxed and are numbered according to the sequence of *Bl*TreA. Active-site residues, Asp203 and Asp329, are located by asterisks. Some representative chloride-independent enzymes are also shown below the line. Symbols denote: *Bl*TreA, *B. licheniformis* TreA (Uni-Prot Acc. No.: Q65MI2); PPA, porcine pancreatic α-amylase (P00690); HAA, human salivary α-amylase (P04745); HPA, human pancreatic α-amylase (P04746); AHA, *Pseudoalteromonas haloplanktis* α-amylase (PZ9957); TMA, *Tenebrio molitor* α-amylase (P56634); *Bs*TreA, *Bacillus subtilis* TreA (P39795); *Ec*TreC, *Escherichia coli* TreC (P28904); *Bc*Ogl, *Bacillus cereus* oligo-1,6-glucosidase (P21332); *Ba*Amy, *Bacillus amyloliquefaciens* α-amylase (P00692); Barley, α-amylase of barley seeds, low pI isozyme AMY-1 (P00693); TAA, α-amylase of *Aspergillus oryzae* (P0C1B3). (b) Local modelled structures around the active-site centre of *Bl*TreA. Residues Arg201, Asp203, Asn327, Asp329 and Tyr365, water molecules (cyan circles), and chloride ion (red circle) are shown. The hydrogen bonds are indicated by dashed lines.

Ramasubbu et al. 1996). These protein ligands coordinated to chloride ion are part of highly conserved regions of Cl^--dependent group of the family GH13 enzymes (Fig. 1a). Notably, the primary difference between the amino acid sequences of Cl^--required α-amylases and those of Cl^--independent enzymes is the K/R337Q/Y substitution. Investigations on *Pseudoalteromonas haloplanctis* α-amylase have demonstrated that chloride ion is not bound by K337R and the starch-degrading ability of this variant is consequently independent of Cl^- (Feller et al. 1996).

Very recently, we have constructed a chimeric plasmid for the functional expression of *Bacillus licheniformis* trehalose-6-phosphate hydrolase (*Bl*TreA) in recombinant *Escherichia coli* (Chuang et al. 2012). The recombinant enzyme is active towards its natural substrate, trehalose-6-phosphate, and quite stable in the presence of organic solvents. Moreover, phylogenetic analysis shows that *Bl*TreA can be classified as a member of the family GH13. Given that the Cl^--binding residues, Arg195, Asn298 and Arg337, have been determined in porcine pancreatic α-amylase (PPA), we aligned the primary structure of *Bl*TreA with those of Cl^--dependent and independent GH13 α-amylases and found that the Arg195 and Asn298 residues of PPA are highly conserved among the compared en-

Table 1. Overlapping complementary primers used in site-directed mutagenesis of *Bl*TreA.

Protein	Nucleotide sequence[a] (5' → 3')	Condon change
R201Q	f- ATCGACGGCTTCCAGCTTGATGTCATC r- GATGACATCAAGCTGGAAGCCGTCGAT	AGA → CAG
R201E	f- ATCGACGGCTTCGAACTTGATGTCATC r- GATGACATCAAGTTCGAAGCCGTCGAT	AGA → GAA
R201K	f- ATCGACGGCTTCAAACTTGATGTCATC r- GATGACATCAAGTTTGAAGCCGTCGAT	AGA → AAA
N327Q	f- TTGTTCTGGTGCCAGCACGACCAGCCG r- CGGCTGGTCGTGCTGGCACCAGAACAA	AAC → CAG
N327D	f- TTGTTCTGGTGCGACCACGACCAGCCG r- CGGCTGGTCGTGGTCGCACCAGAACAA	AAC →GAC
N327K	f- TTGTTCTGGTGCAAACACGACCAGCCG r- CGGCTGGTCGTGTTTGCACCAGAACAA	AAC → AAA
Y365A	f- ACGCCATACATTGCGCAGGGAGAAGAG r- CTCTTCTCCCTGCGCAATGTATGGCGT	TAC → GCG
Y365R	f- ACGCCATACATTCGTCAGGGAGAAGAG r- CTCTTCTCCCTGACGAATGTATGGCGT	TAC → CGT

[a] The altered codons are underlined.

zymes (Fig. 1a). The corresponding residues of *Bl*TreA are Arg201, Asn327, and Tyr365; however, their role in *Bl*TreA has not been investigated. In this study, mutations were introduced into these putative Cl^--binding residues by a commercially available mutagenesis kit. The experimental results indicate that amino acid residues Arg201, Asn327, and Tyr365 are critical for chloride ion binding of *Bl*TreA.

Material and methods

Chemicals

Oligonucleotide primers for the replacement mutations were provided by Mission Biotechnology Inc. (Taipei, Taiwan). Isopropyl-β-D-thiogalactopyranoside (IPTG), antibiotics, *p*-nitrophenyl-α-D-glucopyranoside (*p*NPG) and *p*-nitrophenol (*p*NP) were obtained from Sigma-Aldrich Chemicals (St. Louis, MO, USA). Nickel-nitrilotriacetate (Ni-NTA) resin for protein purification was acquired from Qiagen Inc. (Valencia, CA, USA). Protein assay reagents and chemicals for gel electrophoresis were purchased from Bio-Rad Laboratories (Hercules, CA, USA). Other chemicals were of reagent grade or the equivalent.

Site-directed mutagenesis

The *treA* gene encoding a recombinant *Bl*TreA with a His tag at its N-terminal end was employed as the DNA template (Chuang et al. 2012). For site-directed mutagenesis, eight pairs of complementary mutagenic primers were used for the substitution mutation of Arg201, Asn327, and Tyr365 residues (Table 1). Mutations were created in the *treA* gene using QuikChange II site-directed mutagenesis kit (Stratagene, La Jolla, CA, USA) according to the instructions of the supplier. After a thermocycling program described elsewhere (Lin et al. 2011), the amplified products were treated with *Dpn* I at 37℃ for 1 h to remove unmutated DNA template and were subsequently introduced into competent cells of *Escherichia coli* XL-1 Blue by the $CaCl_2$-mediated transformation process (Mandel & Higa 1970). The transformed cells were thoroughly spread on Luria-Bertani (LB) agar plates containing antibiotic kanamycin (30 μg/mL) and incubated at 37℃ for 18 h. Colonies were randomly picked up for plasmid DNA preparation. Site-specific mutation in each plasmid was verified by DNA sequencing. The verified plasmids were then transformed into *E. coli* M15 (pREP4) host strains for IPTG-induced expression of mutant enzymes.

Enzyme expression and purification

To overexpress *Bl*TreA and its variants, *E. coli* M15 host cells harbouring pQE-*Bl*TreA (Chuang et al. 2012) or each of the mutated plasmids were grown in 100-mL LB medium containing ampicillin (100 μg/mL) and kanamycin (25 μg/mL) at 37℃. Recombinant cells were induced with 10 μM IPTG at an optical density of 0.8 at 600 nm. After cultivation at 28℃ for 12 h, the IPTG-induced cells were harvested by centrifugation at 6,000×*g* for 20 min. The cell pellet was washed twice with 6 mL of Hepes-NaOH buffer (pH 8.0) containing 10 mM imidazole and 0.5 M NaCl, and thereafter resuspended in 12 mL of the same buffer. The resuspended cells were sonicated for 5 min with 30-s rests on ice between each burst, and the lysate sample was clarified by centrifugation (12,000×*g* for 10 min). The crude extract was then subjected to protein purification under native conditions with high-affinity Ni-NTA resin (Chuang et al. 2012). The elution fractions were pooled and dialyzed against 50 mM Hepes-NaOH buffer (pH 8.0) using a 10-kDa cutoff Ultracel-PL membrane (Amicon) for the removal of salts.

Gel electrophoresis and determination of protein concentration

SDS-PAGE was performed on a 12% polyacrylamide slab gel using a discontinuous buffer system (Laemmli 1970). Before gel electrophoresis, the protein samples were dissolved in 1×SDS-PAGE loading buffer (0.1% bromophenol blue, 2% SDS, 5% 2-mercaptoethanol, and 10% glycerol in 50 mM Tris-HCl buffer; pH 6.8) and the resulting suspensions were subsequently boiled for 5 min. Electrophoresis was carried out at a constant voltage of 100 V for 2 h. The electrophoresed gels were stained with coomassie brilliant blue R-250 and destained in a solution of methanol (30%) – acetic acid (10%). Protein molecular weight markers consisted of 97.4 kDa phosphorylase *b*, 66.3 kDa bovine serum albumin, 45.0 kDa ovalbumin, 31.0 kDa carbonic anhydrase, 21.5 kDa trypsin inhibitor, and 14.4 kDa hen egg lysozyme.

Protein concentrations were determined by the Bio-Rad protein assay reagent and bovine serum albumin was used as the concentration reference standard.

Assay for TreA activity
TreA activity was assayed as described previously (Rimmele & Boos 1994) using *p*NPG as an enzyme substrate. The reaction mixture (1 mL) consisted of 5 mM *p*NPG, 100 mM NaCl, 50 mM Hepes-NaOH buffer (pH 8.0), and a suitable dilution (∼9.1 μg/mL) of the enzyme. After 10-min incubation at 30 °C, the hydrolysis of *p*NPG was terminated by boiling the reaction mixture for 5 min. The heated sample was leaved for 5–10 min until cooled to room temperature and the absorbance at 410 nm (A_{410}) of the supernatant was measured. One unit of *Bl*TreA activity is defined as the amount of enzyme that produces 1 μmol of *p*NP per min at 30 °C.

A steady-state kinetics study of *Bl*TreA was carried out at 30 °C in 50 mM Hepes-NaOH buffer (pH 8.0) containing 100 mM NaCl and a range of *p*NPG concentrations (0.1–10.2 mM). Kinetic parameters were estimated from least-squares fit of initial rates as a function of substrate concentration. Value of k_{cat}/K_M was calculated from the slope of the linear part of the Michaelis-Menten plot at substrate concentrations less than K_M.

To determine the effect of NaCl on the TreA activity, the purified enzymes were further desalted by PD10 desalting column (GE Healthcare, Buckinghamshire HP7 9NA, UK). Thereafter, TreA activity was assayed at 30 °C for 10 min with a reaction mixture of 5 mM *p*NPG, 50 mM Hepes-NaOH buffer (pH 8.0), an appropriate volume of enzyme solution, and different concentrations of NaCl.

Monovalent ion titration of apo-enzymes
Cl^--free wild-type and mutant enzymes were prepared by gel filtration on a Sephadex G-25 column with an elution buffer of 50 mM Hepes-NaOH (pH 8.0). The dissociation constants for monovalent ions were calculated from the activation curves generated by NaF, NaCl, $NaNO_3$, LiCl, KCl, and RbCl titration in the *p*NPG reaction mixture. The data points were computer-fitted with a nonlinear regression analysis of the Hill equation (Eq. 1):

$$v = k_{cat}[A]_H^n/K_d + [A]_H^n \quad (1)$$

where k_{cat} is the catalytic turnover number, [A] is the monovalent ion concentration, n_H is the Hill coefficient, and K_d is the dissociation constant.

Spectral analyses
Far-UV circular dichroism (CD) studies were carried out by a JASCO-815 spectrometer (JASCO Inc., Japan) equipped with the temperature control system of liquid nitrogen. Samples were adjusted with 5 mM Hepes-NaOH buffer (pH 8.0) to a protein concentration of approximately 0.132 mg/mL before the spectral analyses. Far-UV CD spectra were recorded over the wavelength range of 190–250 nm using a 1-mm path length cell. The absorbance of photomultiplier was carefully kept below 600 V during the analysis. Ten spectra were averaged for each sample and the obtained data were carefully corrected by subtracting buffer contribution from the parallel spectra in the absence of protein. The data were expressed as molar ellipticity (deg cm^2 $dmol^{-1}$) based on a residue number of 562 and a mean residue weight (MRW) of 65.8 kDa. Molar ellipticity was calculated as $[\theta] = [100 \times (MRW) \times \theta_{obs}/(c \times l)]$, where θ_{obs} represents the observed ellipticity in degree at a given wavelength, c is the protein concentration in mg/mL, and l is the length of the light path in cm.

Thermal unfolding of wild-type and mutant proteins (0.158 mg/mL) in 5 mM Hepes-NaOH buffer (pH 8.0) was monitored by recording the change in ellipticity at 222 nm. Protein samples were heated at a scan rate of 2 °C/min. The changes in ellipticity (θ) at 222 nm were analyzed according to the equation as described elsewhere (Greenfield 2004).

The fluorescence emission analysis of wild-type and mutant enzymes was performed by a JASCO FP-6500 fluorescence spectrophotometer (JASCO Inc., Japan) with an excitation wavelength of 295 nm. All spectra were corrected for the contribution of 5 mM Hepes-NaOH buffer (pH 8.0). Samples were diluted to a protein concentration of 7.1 μg/mL by 5 mM Hepes-NaOH buffer (pH 8.0) and their fluorescence emission spectra were collected with a scanning speed of 240 nm/min and a response time of 1 s. The maximal peak of fluorescence spectra and the changes in fluorescence intensity were used to evaluate the unfolding of wild-type and mutant proteins.

Structural modelling
Computer modelling of *Bl*TreA was conducted to identify the interactions between the target residues and the chloride ion. The molecular structures of *Bl*TreA and its variants were essentially constructed at SWISS MODEL Server using X-ray crystal structures of *Bacillus cereus* oligo-1,6-glucosidase (*Bc*Ogl) (PDB code: 1UOK) and porcine pancreatic α-amylase (PDB code: 1BVN), and the model molecular structures were further energy minimized by the usage of CNS program (http://cns.csb.yale.edu/v1.1/).

Results and discussion

Sequence comparison and molecular modelling
Among the family GH13 enzymes, one group is allosterically activated by the binding of chloride ion. These Cl^--dependent α-amylases are usually specific to all mammalian species, but are also found in a few types of bacteria, such as *Pseudoalteromonas haloplanktis* (D'Amico et al. 2000). The solved structures of chloride-dependent α-amylases from human salivary (Ramasubbu et al. 1996) and pancreatic (Brayer et al. 1995) glands, porcine pancreas (Qian et al. 1993; Larson et al. 1994), *Tenebrio molitor* (Strobl et al. 1998), and *P. haloplanktis* (Aghajari et al. 2002) contain the ion at a common site, which is located close to the center of the $(\beta/\alpha)_8$-barrel and in the near vicinity of the catalytic site. The protein ligands for the chloride ion and the interaction network within the active site have been elucidated (Aghajari et al. 2002).

Amino acid sequences of *Bl*TreA and five chloride-dependent α-amylases and six representative chloride-independent enzymes were aligned by the program BLASTX. *Bl*TreA exhibits a highest sequence identity (70.3%) with *Bc*Ogl but the overall sequence identity to other counterparts was between 13.3 and 54.1%. As shown in Figure 1a, the chloride-coordinated residues Arg195 and Asn298 (numbering in PPA) are conserved in Cl^--dependent α-amylases and are therefore the key feature for the binding of anion (Feller et al. 1996; D'Amico et al. 2000). Another arginine acts as the third ligand, which is substituted by a lysine, tyrosine, glutamine, cysteine or isoleucine residue in microbial α-amylases. The corresponding residues of *Bl*TreA are Arg201, Asn327, and Tyr365 (Fig. 1a). The situation

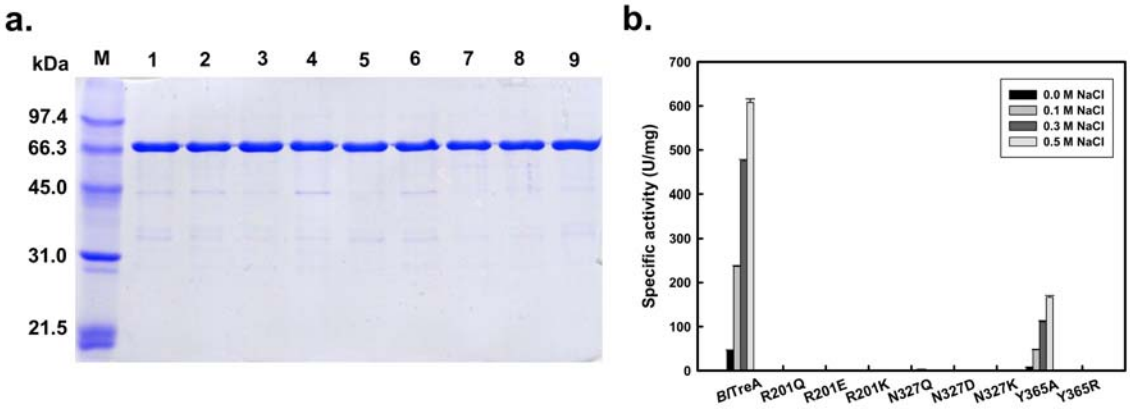

Fig. 2. SDS-PAGE analysis (a) and specific activity (b) of *Bl*TreA and its variants. Lanes: M, protein size markers; 1, *Bl*TreA; 2, R201Q; 3, R201E; 4, R201K; 5, N327Q; 6, N327D; 7, N327K; 8, Y365A; 9, Y365R.

of conserved Arg201, Asn327, and Tyr365 residues at the putative Cl^--binding site of *Bl*TreA warranted their exploration as the crucial residues for the coordination of chloride ion (Fig. 1b).

Enzymatic characterization of wild-type and mutant proteins

Following gene expression and protein purification, *Bl*TreA and its variants were subjected to SDS-PAGE (Fig. 2a). Gel electrophoresis results indicated over 95% purity after the affinity chromatography and the identical molecular mass ($\sim$ 65.9 kDa) for all proteins. Based on the equivalent yields for wild-type and mutant enzymes, we would argue against the errant folding and stability of these proteins during IPTG-induced expression and the subsequent purification. To examine whether changes to the TreA activity occurred as a result of the replacements, the enzymatic activity of *Bl*TreA and its variants was assayed. The purified *Bl*TreA had a specific activity of 236.9 U/mg protein, and the K_M and k_{cat} values of the recombinant enzyme were determined to be 5.4 ± 0.7 mM and 31.9 ± 4.3 s^{-1}, respectively. The TreA activity of Y365A was profoundly reduced to 47.6 U/mg protein with a catalytic efficiency of 1.2 s^{-1} mM^{-1}. Furthermore, a complete loss of the TreA activity was observed for the remaining variants. It is worth to mention that the desalted *Bl*TreA and Y365A enzymes were less effective towards *p*NPG, retaining lower than 15.8% of the TreA activity (Fig. 2b). Their enzymatic activity was activated by 5.2–22.3 fold upon the addition of 0.1–0.5 M NaCl. However, NaCl did not significantly activate the TreA activity of the remaining mutant enzymes. These results suggest that chloride ion has a stimulatory effect on the *Bl*TreA activity and the putative chloride-binding residues are critical for the proper function of the enzyme.

Binding of monovalent ions

Functional role of chloride ion has been proposed according to the currently accepted reaction mechanism of glycosidases (McCarter & Withers 1994) and the crystallographic studies of cyclodextrin glycosyltransferase (Strokopytov et al. 1995) and α-amylase (Qian et al. 1994). These glycosidases require a protonated side chain acting as a general acid catalyst that donates a proton to the weakened glycosidic bond. This side chain has been identified as Glu257 in the CGTase and Glu233 in the α-amylase. Interestingly, Ca^{2+} inhibition of two *Aspergillus* α-amylases arises from the binding of a second Ca^{2+} ion to the carboxyl group of Glu233 in a bidentate mode and of Asp197 in a unidentate mode (Boel et al. 1990). A study of *P. haloplanctis* α-amylase has revealed that Cl^- can interact with active site carboxylates and the protective effect against Ca^{2+} inhibition is consistent with the appearance of a protonated carboxyl group upon Cl^- binding (Feller et al. 1996). The chloride-binding site of mammalian pancreatic and salivary α-amylases consists of Arg195, Asn298, the side-chain amines of Arg337, and a water molecule (Brady et al. 1991; Qian et al. 1993; Lawson et al. 1994; Ramasubbu et al. 1996). This binding site of *Bl*TreA differs from them by a tyrosine residue instead of Arg337 (Fig. 1a). Removal of chloride ion by gel filtration led to the reversible inactivation of *Bl*TreA and Y365A. These two enzymes were fully activated by chloride ion (Fig. 3a) and displayed a K_d value of 106.1 $\pm$ 10.1 and 254.3 $\pm$ 31.2 mM, respectively at 25 ℃. Hill coefficient (n_H) for each titration was close to 1.0, indicating that only one anion is bound during the titration. Despite of there is no direct relation between the K_d value and the activation capacity, *Bl*TreA and Y365A could also bind to F^- and NO_3^- anions with a K_d value of $119.8 \pm 14.9/94.7 \pm 7.4$ and $264.1 \pm 46.2/155.1 \pm 7.1$ mM, respectively (Fig. 3b and c). However, as a control, these three anions did not exhibit any activation on Y365R. Mutations of Arg201 and Asn327 to other residues caused a complete loss of the TreA activity and these variants were obviously devoid of the anion-binding ability. These results reveal that the anion-binding site of *Bl*TreA cannot accommodate the side chains of the substituted residues in the appropriate orientations.

Effect of monovalent cations on the reversible activation of wild-type and mutant apo-enzymes was also investigated. As shown in Figure 3, the monovalent

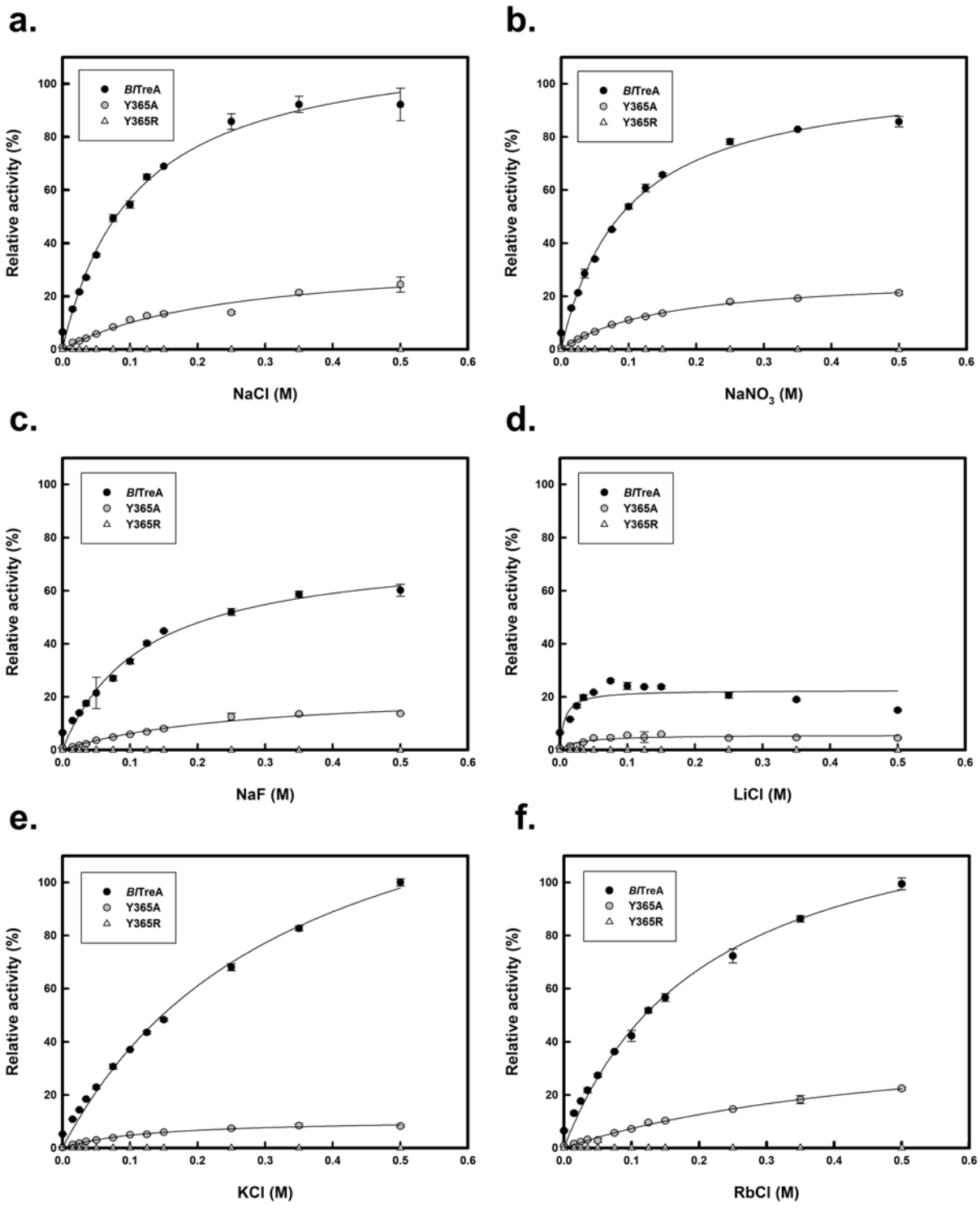

Fig. 3. Titration of *Bl*TreA, Y365A, and Y365R by monovalent ions. The solid lines depict parabolic fits to each profile. The enzymatic activity of *Bl*TreA titrated with 0.5 M KCl was taken as 100%.

cations (Li^+, Na^+, K^+ and Rb^+) did not seem to play a major role in the reactivation of wild-type and mutant apo-enzymes. These findings together with the titration data of F^-, Cl^- and NO_3^- anions clearly indicate that cation is not an essential part of the catalytic reaction of *Bl*TreA.

Spectral studies of BlTreA and its variants

To evaluate how the secondary structural elements of *Bl*TreA were affected by the mutations, we analyzed far-UV CD spectral profiles of *Bl*TreA and its variants. The far-UV CD spectrum of *Bl*TreA had strong peaks of negative ellipticity at both 208 and 222 nm, which is an indicative of a substantial α-helical content (Fig. 4a). The spectrometric characteristic of all mutant enzymes strongly resembled those of *Bl*TreA. These observations indicate that no notable change in the secondary structural

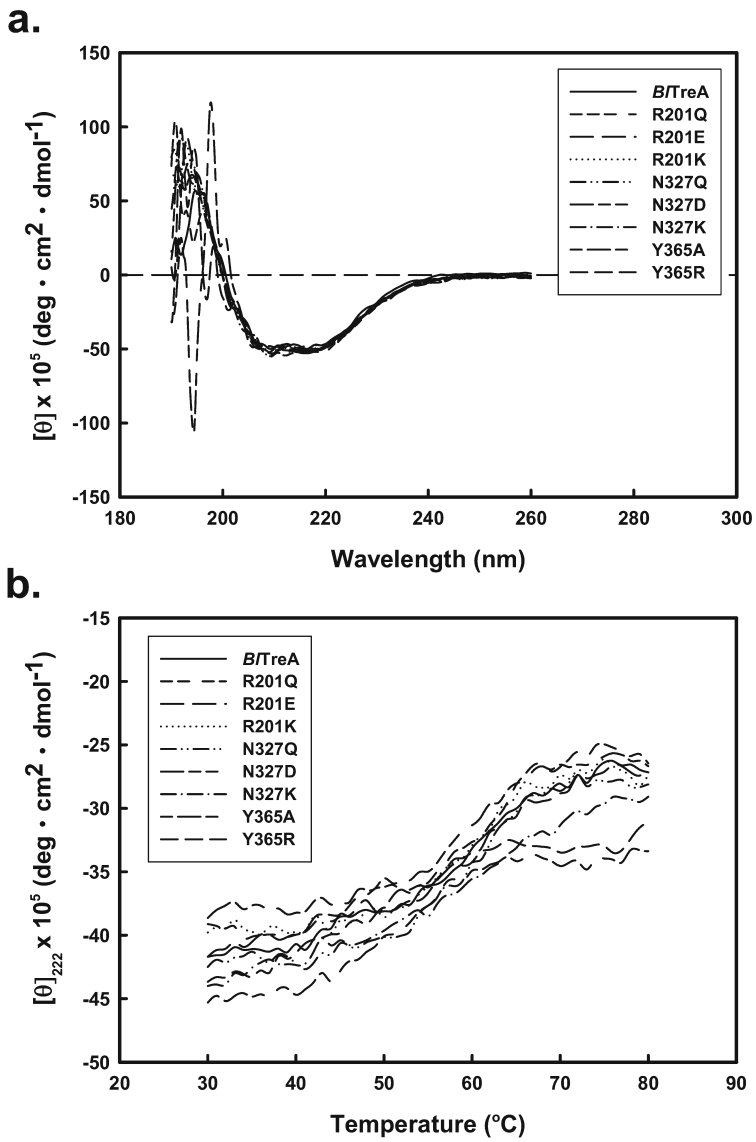

Fig. 4. CD analysis of wild-type and mutant enzymes. (a) Far-UV spectra of *Bl*TreA and its variants. The data were recorded at 22 °C and residual molar ellipticities of the protein samples in 5 mM Hepes-NaOH buffer (pH 8.0) were measured from 190-260 nm. (b) Thermal denaturation of *Bl*TreA and its variants. The protein samples in 5 mM Hepes-NaOH buffer (pH 8.0) were monitored with the CD signal at 222 nm.

elements of *Bl*TreA has occurred after the mutations.

Thermal unfolding transitions of *Bl*TreA and its variants followed by the loss of ellipticity at 222 nm with the temperature increment was also investigated (Fig. 4b). The transition for *Bl*TreA started at about 40.7 °C and had a midpoint of 58.1 °C. The T_m value (57.8–59.1 °C) for all variants was close to that of the wild-type enzyme. These results clearly indicate that replacements of Arg201, Asn327, and Tyr365 with other amino acids do not have a significant effect on the thermal stability of *Bl*TreA.

Fluorescence emission spectra provide a sensitive way to analyze proteins and their respective conformations. The spectrum is determined mainly by the polarity of the microenvironment of the tryptophan residues and by their specific interactions (Royer 2006). Based on this principle, tryptophan fluorescence emission spectrum of *Bl*TreA was characterized by a peak centred at 331.4 nm (Fig. 5). The variants had fluorescence emission spectra qualitatively consistent with that of the wild-type protein. However, the fluorescence intensity of mutant proteins was either quenched by 2.6–8.1% or enhanced by 0.3–4.4% with respect to *Bl*TreA. These observations suggest that the amino acid replacements at positions 201, 327, and 365 cause minor structural changes in the enzyme.

Structural interpretation

Sequence alignment of *Bl*TreA with Cl^--dependent and independent family GH13 enzymes allows us to identify the critical residues potentially involved in the coordination of the chloride ion. As shown in Figure 1a, the putative protein ligands for the coordination of *Bl*TreA to the chloride ion are Arg201, Asn327, and Tyr365. Although the primary structure of *Bl*TreA is highly ho-

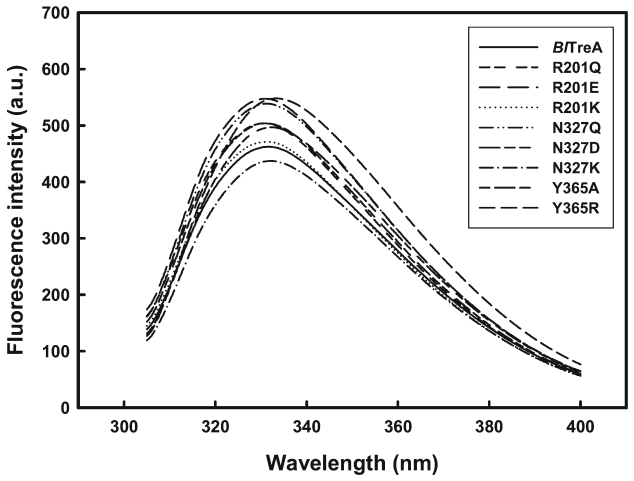

Fig. 5. Intrinsic fluorescence spectra of *Bl*TreA and its variants. An average of five spectra for each protein sample was recorded.

mologous to that of *Bc*Ogl and the crystal structure (1UOK) of this counterpart is available since 1999, the Cl^--free structure is not suitable for use as the template to model the putative chloride-binding site of *Bl*TreA. With PPA as the structural template, the local environment surrounding the Cl^- ion was modelled for the wild-type enzyme. As shown in Figure 1b, both modelled structures around the active-site centre of *Bl*TreA are similar with the exception of the tyrosine's position at 365. There are several interactions between the putative chloride-binding residue Arg201 and its surrounding residues (Fig. 1b), in which Met100 OA interacts with Arg201 NB, Leu102 NB interacts with Arg201 OA, and Asp101 OD1 and OD2 and Asp203 OD interact with Arg201 NH1, Asp248 OD and the chloride ion interacts with Arg201 NH2. For another putative chloride-binding residue Asn327, its OA interacts with Pro331 NZ and Gln330 NB, and ND of this residue interacts with His299 NE, the water molecule and the chloride ion. Asn327 OD also interacts with the water molecule. These interactions might play an important role for the position of the chloride ion at the putative active site of *Bl*TreA. Although Tyr365 OA interacts with Gln366 NE and its NB is hydrogen-bonded to Ala323 OA, this residue seems not to be directly coordinated with the chloride ion (Fig. 1b). Based on the modelled structure, the loss of correct ligand Cl^- conformations in the mutant proteins, especially those of Arg201 and Asn347 mutations, could be the reason for their inability to act on the enzyme substrate.

Because*Bl*TreA and the PPA template share only 13.3% sequence identity, crystallization of the wild-type protein is a promising way for the structural elucidation of residues Arg201, Asn327 and Tyr365. Three-dimensional structure determination of *Bl*TreA is currently in progress and the resultant structure would provide useful information toward a more comprehensive understanding of the influence of chloride on the activity of this enzyme.

Conclusions

The protein ligands for the coordination of chloride ion belong to highly conserved sequence regions of the family GH13 enzymes. Residues Arg201 and Asn327 of *Bl*TreA are invariably located at the -2 position with respect to the catalytic nucleophile Asp203 and the essential Asp329. The basic residue Arg/Lys337 of Cl^--dependent α-amylases is replaced by a tyrosine, glutamine, cysteine or isoleucine residue in Cl^--independent enzymes (Fig. 1a) and mutations in the corresponding residue reveal that the third ligand appears to be a non-critical component for the Cl^--binding of *Bl*TreA. To the best of our knowledge, this is the first report dealing with the mutational impact of the putative chloride-binding residues to a bacterial trehalose-6-phosphate hydrolase. The experimental evidence would provide new insights into the ligand-Cl^- coordination of the GH13 family enzymes of microbial origin.

Acknowledgements

The present work was supported by grants from National Science Council of Taiwan (NSC 97-2628-B-415-001-MY3 and NSC 100-2313-B-415-003-MY3).

References

Aghajari N., Feller G., Gerday C. & Haser R. 1998. Crystal structure of the psychrophilic α-amylase from *Alteromonas haloplanctis* in its native form and complexed with an inhibitor. Protein Sci. **7:** 564–572.

Aghajari N., Feller G., Gerday C. & Haser R. 2002. Structural basis of α-amylase activation by chloride. Protein Sci. **11:** 1435–1441.

Boel E., Brady L., Brzozowsi A.M., Derewenda Z., Dodson G.G., Jensen V.J., Petersen S.B., Swift H., Thim L. & Woldike H.F. 1990. Calcium binding in α-amylases: an X-ray diffraction study at 2.1-Å resolution of two enzymes from *Aspergillus*. Biochemistry **29:** 6244–6249.

Brady R.L., Brzozowski A.M., Derewenda Z.S., Dodson E.J. & Dodson G.G. 1991. Solution of the structure of *Aspergillus niger* acid α-amylase by combined molecular replacement and multiple isomorphous replacement methods. Acta Crystallogr. **B47:** 527–535.

Brayer G.D., Luo Y. & Withers S.G. 1995. The structure of human pancreatic α-amylase at 1.8 Å resolution and comparisons with related enzymes. Protein Sci. **4:** 1730–1742.

Chuang T.T., Ong P.L., Wang T.F., Huang H.B., Chi M.C. & Lin L.L. 2012. Molecular characterization of a novel trehalose-6-phosphate hydrolase, TreA, from *Bacillus licheniformis*. Int. J. Biol. Macromol. **50:** 459–470.

D'Amico S., Gerday C. & Feller G. 2000. Structural similarities and evolutionary relationships in chloride-dependent α-amylases. Gene **253:** 95–105.

Greenfield N.J. 2004. Analysis of circular dichroism data. Methods Enzymol. **383:** 282–317.

Feller G., le Bussy O., Houssier C. & Gerday C. 1996. Structural and functional aspects of chloride binding to *Alteromonas haloplanctis* α-amylase. J. Biol. Chem. **271:** 23836–23841.

Feller G., Lonhieme T., Deroanne C., Libioulle C., van Beeumen J. & Gerday C. 1992. Purification, characterization, and nucleotide sequence of the thermolabile α-amylase from the antarctic psychrotroph *Alteromonas haloplanctis* A23. J. Biol. Chem. **267:** 5217–5221.

Feller G., Payan F., Theys F., Qian M., Haser R. & Gerday C. 1994. Stability and structural analysis of α-amylase from the

Antarctic psychrophilic *Altermonas haloplanctis* A23. Eur. J. Biochem. **222:** 441–447.

Henrissat B. 1991. A classification of glycosyl hydrolases based on amino-acid sequence similarities. Biochem. J.**280:** 309–316.

Henrissat B. & Bairoch A. 1996. Updating the sequence-based classification of glycosyl hydrolases. Biochem. J. **316:** 695–696.

Janeček Š. 1994. Parallel β/α-barrels of α-amylase, cyclodextrin glycosyltransferase and oligo-1,6-glucosidase versus the barrel of β-amylase: evolutionary distance is a reflection of unrelated sequences. FEBS Lett. **353:** 119–123.

Janeček Š. 1995. Close evolutionary relatedness among functionally distantly related members of the $(\beta/\alpha)_8$-barrel glycosyl hydrolases suggested by the similarity of their fifth conserved sequence region. FEBS Lett. **377:** 6–8.

Jespersen H.M., MacGregor E.A., Henrissat B., Sierks M.R. & Svensson B. 1993. Starch- and glycogen-debranching and branching enzymes: prediction of structural features of the catalytic $(\beta/\alpha)_8$-barrel domain and evolutionary relationship to other amylolytic enzymes. J. Protein Chem. **12:** 791–805.

Kadziola A., Abe J., Svensson B. & Haser R. 1994. Crystal and molecular structure of barley α-amylase. J. Mol. Biol. **239:** 104–121.

Kizaki H., Hata Y., Watanabe K., Katsube Y. & Suzuki Y. 1993. Polypeptide folding of *Bacillus cereus* ATCC7064 oligo-1,6-glucosidase revealed by 3.0 Å resolution X-ray analysis. J. Biochem. **113:** 646–649.

Klein C. & Schulz G.E. 1991. Structure of cyclodextrin glycosyltransferase refined at 2.0 Å resolution. J. Mol. Biol. **217:** 737–750.

Knegtel R.M.A., Wind R.D., Rozeboom H.J., Kalk K.H., Buitelaar R.M., Dijkhuizen L. & Dijkstra B.W. 1996. Crystal structure at 2.3 Å resolution and revised nucleotide sequence of the thermostable cylodextrin glycosyltransferase from *Thermoanaerobacterium thermosulfurigenes* EM1. J. Mol. Biol. **256:** 611–622.

Kubota M., Matsuura Y., Sakai S. & Katsube Y. 1991. Molecular structure of *B. stearothermophilus* cyclodextrin glucanotransferase and analysis of substrate binding site. Denpun Kagaku **38:** 141–146.

Laemmli U.K. 1970. Cleavage of structural proteins during the assembly of the head of bacteriophage T4. Nature **227:** 680–685.

Larson S.B., Greenwood A., Cascio D., Day J. & McPherson A. 1994. Refined molecular structure of pig pancreatic α-amylase at 2.1 Å resolution. J. Mol. Biol. **235:** 1560–1584.

Lawson C.L., van Montfort R., Strokopytov B., Rozeboom H.J., Kalk K.H., de Vries G.E., Penninga D., Dijkhuizen L. & Dijkstra B.W. 1994. Nucleotide sequence and X-ray structure of cyclodextrin glycosyltransferase from *Bacillus circulans* strain 251 in a maltose dependent crystal form. J. Mol. Biol. **236:** 590–600.

Lin M.G., Liang W.C., Chen B.E., Chou W.M. & Lin L.L. 2011. Involvement of residues Asp8, Asn13, Glu145, Asp168, and Thr173 in the chaperone activity of a recombinant DnaK from *Bacillus licheniformis*. J. Mol. Microbiol. Biotechnol. **20:** 29–42.

McCarter J.D. & Withers S.G. 1994. Mechanisms of enzymatic glycoside hydrolysis. Curr. Opin. Struct. Biol. **4:** 885–892.

MacGregor E.A. 1993. Relationships between structure and activity in the α-amylase family of starch-metabolising enzymes. Starch/Stärke **7:** 232–237.

Machius M., Wiegand G. & Huber R. 1995. Crystal structure of calcium depleted *Bacillus licheniformis* α-amylase at 2.2 Å resolution. J. Mol. Biol. **246:** 545–559.

Mandel M. & Higa A. 1970. Calcium-dependent bacteriophage DNA infection. J. Mol. Biol. **53:** 159–162.

Matsuura Y., Kusunoki M., Harada W. & Kakudo M. 1984. Structure and possible catalytic residues of Taka-amylase A. J. Biochem. **95:** 697–702.

Qian M., Haser R., Buisson G., Duee E. & Payan F. 1994. The active center of a mammalian α-amylase: structure of the complex of a pancreatic α-amylase with a carbohydrate inhibitor refined to 2.2-Å resolution. Biochemistry **33:** 6284–6294.

Qian M., Haser R. & Payan F. 1993. Structure and molecular model refinement of pig pancreatic α-amylase at 2.1 Å resolution. J. Mol. Biol. **231:** 785–799.

Ramasubbu N., Paloth V., Luo Y., Brayer G.D. & Levine M.J. 1996. Structure of human salivary α-amylase at 1.6 Å resolution: implications for its role in the oral cavity. Acta Crystallogr. **D52:** 435–446.

Rimmele M. & Boos W. 1994. Trehalose-6-phosphate hydrolase of *Escherichia coli*. J. Bacteriol. **176:** 5654–5664.

Royer C.A. 2006. Probing protein folding and conformational transitions with fluorescence. Chem. Rev. **106:** 1769–1784.

Strobl S., Maskos K., Betz M., Wiegand G., Huber R., Gomis-Ruth F.X. & Glockshuber R. 1998. Crystal structure of yellow meal worm α-amylase at 1.64 Å resolution. J. Mol. Biol. **278:** 617–628.

Strokopytov B., Penninga D., Rozeboom H.J., Kalk K.H., Dijkuizen L. & Dijkstra B.W. 1995. X-ray structure of cyclodextrin glycosyltransferase complexed with acarbose: implications for the catalytic mechanism of glycosidases. Biochemistry **34:** 2234–2240.

Svensson B. 1994. Protein engineering in the α-amylase family: catalytic mechanism, substrate specificity, and stability. Plant Mol. Biol. **25:** 141–157.

Watanabe K., Hata Y., Kizaki H., Katsube Y. & Suzuki Y. 1997. The refined structure of *Bacillus cereus* oligo-1,6-glucosidase at 2.0 Å: structural characterization of proline-substituted sites for protein stabilization. J. Mol. Biol. **269:** 142–153.

Received March 28, 2013
Accepted July 30, 2013